# Shear Alignment Mechanisms of Close-Packed Spheres in a Bulk ABA Triblock Copolymer

Wenyue Ding,<sup>a</sup> Josiah Hanson,<sup>a</sup> Wesley R. Burghardt,<sup>b</sup> Carlos R. López-Barrón,<sup>c</sup> Megan L. Robertson<sup>ad</sup>\*

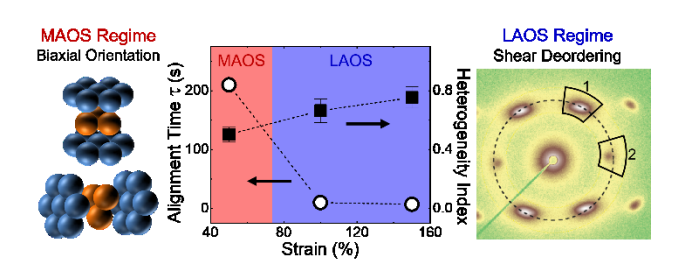
<sup>a</sup> William A. Brookshire Department of Chemical & Biomolecular Engineering, University of Houston, Houston, TX, 77204-4004

<sup>b</sup> Department of Chemical and Biological Engineering, Northwestern University, Evanston, IL,60208

> <sup>c</sup> ExxonMobil Chemical Company, Baytown, TX, 77522 <sup>d</sup> Department of Chemistry University of Houston, Houston, TX 77204-4004

\*Corresponding author Megan Robertson 4226 Martin Luther King Blvd. S222 Engineering Building 1 University of Houston Houston, TX 77204-4004 mlrobertson@uh.edu 713-743-2748

Table of Contents Graphic (for Table of Contents use only)



**KEYWORDS:** small-angle X-ray scattering, Fourier-transform rheology, large amplitude oscillatory shear, face-centered cubic spheres, hexagonally close-packed spheres, poly(*n*-alkyl acrylates), polystyrene, thermoplastic elastomers, shear deordering

#### Abstract

The alignment and shear-induced microstructural changes of closed-packed spheres observed in a poly(styrene-b-lauryl acrylate-b-styrene) triblock copolymer were quantified with a combination of *in situ* small-angle X-ray scattering (SAXS) and Fourier-transform (FT) rheology. Disordered spheres produced through compression molding were transformed to close-packed spheres through the application of nonlinear oscillatory shear. FT-rheology identified strain amplitude regimes for small-, medium-, and large-amplitude oscillatory shear behaviors (SAOS, MAOS, and LAOS, respectively), at fixed temperature and frequency. The presence of oscillatory shear induced orientational changes in the hexagonally-closed packed (HCP) layers. Increasing the strain amplitude produced faster ordering and higher degree of orientation, quantified through fitting a stretched exponential function to in situ SAXS and FT-rheology data. In the MAOS regime, shear thinning behavior was observed, with decrease in the storage modulus (G') due to the formation of HCP layers that exhibited less resistance to flow. The third order harmonic  $(I_{3/1})$ increased with the square of the strain amplitude, hypothesized to originate from the presence of sharp grain interphase boundaries (due to defects), and Chebyshev coefficients indicated intracycle shear thickening and strain stiffening. In the LAOS regime, HCP layers adopted a parallel orientation with a zig-zag path sliding mechanism, and both G' and the loss modulus (G") decreased with increasing strain amplitude. Interestingly, at higher strain amplitude, shear deordering was observed, for the first time in close-packed spheres under oscillatory shear, as evidenced by characteristic signatures in both in situ SAXS and FT-rheology data. Structural rearrangements were consistent with the domain dissolution and reformation mechanism.

# Introduction

Block copolymers composed of incompatible components have been extensively studied due to their ability to self-assemble into microphase-separated morphologies, enabling diverse applications spanning membranes, 1 elastomers, 2 blend compatibilizers, 3 and polymer modifiers, among others. This spontaneous self-assembly often leads to the presence of polydomains lacking long range order; however, many applications require highly oriented and aligned domains, such as microelectronics, 4,5 functional membranes, 6 and optical and photovoltaic devices. 7-9 Numerous methods have been developed to align block copolymer domains, such as the application of shear, <sup>10-12</sup> electrical and magnetic fields, <sup>13, 14, 15, 16</sup> zone annealing, <sup>17-19</sup> solvent vapor annealing, <sup>20-</sup> <sup>22</sup> and templated assembly. <sup>23-25</sup> Among these methods, shear alignment has been shown to be a feasible approach to effectively align block copolymer melts and concentrated solutions. Prior studies on the shear alignment of block copolymers with spherical, 26-28 cylindrical, 29-31 gyroid, 32-34 and lamellar<sup>35-38</sup> morphologies, have shown the response of the morphology to shear generally depends on the nature of block copolymer (e.g., architecture, molecular weight and segregation strength) and shear conditions (e.g., temperature, rate of deformation and amplitude of deformation).

The morphological response of lamellae- and cylinder-forming block copolymers to shear has been extensively studied. For both morphologies, three possible orientations can be achieved: perpendicular, parallel, and transverse.  $^{10,35,36,39-42}$  Under shear, the microstructure alignment tends to collectively minimize viscous dissipation and chain mixing.  $^{43}$  In the case of parallel and perpendicular orientations, the concentration gradient between the microdomains is perpendicular to the velocity direction ( $\vec{1}$ ) of the shear flow to prevent intermixing of dissimilar chains. Thus, parallel and perpendicular orientations are more stable than the transverse orientation and are

commonly encountered in lamellar and cylindrical systems. Under certain conditions (e.g. high frequency in oscillatory shear<sup>44</sup> or presence of liquid crystalline domains on the side chain<sup>31, 45</sup>), the transverse orientation can be achieved.

Relatively few reports have appeared on the shear alignment of sphere-forming bulk block copolymers. The predominant lattice formed by spheres in bulk block copolymers is body-centered cubic (BCC).<sup>26, 46, 47</sup> Under shear, the (111) plane in BCC spheres often aligns parallel to the shear direction.<sup>48-55</sup> BCC spheres can transition to hexagonally close-packed systems through the application of high strain<sup>48</sup> and this is often observed in films.<sup>49-51, 53, 56</sup> Spherical morphologies can also adopt complex lattices such as Frank-Kasper phases and dodecagonal quasicrystals, which are induced by conformational asymmetry of the block copolymers.<sup>28, 57-64</sup>

Though the presence of close-packed (CP) spheres is predicted by self-consistent mean-field theory in a narrow region of the bulk block copolymer phase diagram, <sup>65</sup> they are not observed as frequently as the BCC morphology. CP spheres have been reported in bulk block copolymers under quiescent conditions<sup>27, 66, 67</sup> and under extensional flow upon thermal annealing. <sup>68</sup> The absence of broader experimental observations of CP spheres is attributed to disruption of long-range order of CP spheres through thermal fluctuations. <sup>69, 70</sup> Also, the CP spherical phase was shown to be thermodynamically unfavorable, as it is superseded by a disordered micelle phase due to gains in translational entropy. <sup>71</sup> However, the CP spherical morphology can be stabilized by alleviating the packing frustrations of the block copolymer melt by addition of solvent <sup>72-74</sup> or homopolymer, <sup>75, 76</sup> and also by increasing the dispersity. <sup>66, 77</sup> Even small increases in dispersity (< 1.1) are sufficient to stabilize CP spheres, through mechanisms such as presence of interstitial sites and chain pull-out. <sup>66</sup> Recently, our group reported the transformation of a disordered spherical

morphology to CP spheres upon application of shear to a bulk block copolymer melt with higher dispersity.<sup>78</sup>

*In situ* techniques, such as small-angle X-ray scattering, small-angle neutron scattering and birefringence, allow the real-time monitoring of morphological changes in block copolymers during alignment, permitting exploration of kinetic pathways to aligned morphologies. The majority of the literature has demonstrated a monotonic change from an unaligned structure to an aligned structure upon shearing. <sup>26, 37, 74, 79</sup> However, a few studies have shown the presence of shear can cause non-monotonic changes. The orientation of lamellae in a concentrated block copolymer solution changed from isotropic to perpendicular to disordered upon application of shear.<sup>80, 81</sup> Similar behavior was observed in a lamellae-forming block copolymer melt, in which the lamellar orientation transitioned from isotropic to perpendicular and finally to a less-ordered biaxial orientation. 82 These results demonstrate the existence of an intermediate orientational state, and thus orientations reported using ex situ methods may in fact be transient or non-equilibrium states. It is therefore crucially important to monitor the alignment process in situ. Moreover, the orientation and degree of order are governed by the shear protocol (e.g., duration, frequency, temperature and strain amplitude), and a deeper understanding of alignment mechanisms and kinetics allows optimization of the alignment process for targeted application. Even more powerful is the ability to associate morphological changes with underlying mechanical response under nonlinear flow. Recently, Fourier transform (FT)-rheology has been introduced as a tool to quantify the mechanical response to oscillatory shear in the nonlinear region by analysis of higherorder harmonics in the stress response. 83 The relative intensity of the third harmonic (I<sub>3/1</sub>) is sensitive to morphological changes and can be used as a mechanical response parameter to monitor the shear alignment process. 38, 82, 84, 85

Here, we examine the kinetic alignment pathways of a bulk triblock copolymer forming a CP spherical morphology under shear, using *in situ* SAXS and FT-rheology (we previously reported the existence of CP spheres in this system, attributed to the higher dispersity of the midblock<sup>78</sup>). The structural response was correlated to the mechanical response under shear. We report the first observation of shear-induced deordering of CP spheres in a block copolymer melt. At high strain amplitude ( $\gamma = 150\%$ ), a highly ordered close-packed spherical morphology was achieved at short times and then degenerated to a poorly-ordered structure upon further application of shear. The effect of strain amplitude on the orientational behavior of CP spherical layers was evaluated. In the large-amplitude oscillatory shear (LAOS) region, parallel orientation of CP spheres was observed, and in the medium-amplitude oscillatory shear (MAOS) region, a subset of spheres reoriented to a more irregular orientation, producing additional grain defects. Increasing the strain amplitude produced faster ordering and higher degree of orientation. Structural rearrangements were consistent with the domain dissolution and reformation mechanism.

# **Experimental Methods**

#### **Materials**

All chemicals were purchased from Sigma Aldrich unless otherwise noted.

# Synthesis and Characterization of Poly(styrene-b-lauryl acrylate-b-styrene) Triblock Copolymer

Detailed synthetic and characterization procedures were described previously for the preparation of a poly(styrene-b-lauryl acrylate-b-styrene) (SAS) triblock copolymer. <sup>86</sup> Briefly, the SAS triblock copolymer was synthesized through a two-step reversible addition-fragmentation chain transfer polymerization. Proton nuclear magnetic resonance ( ${}^{1}H$  NMR) was performed on a JEOL-500 instrument using deuterated chloroform. The number-average molecular weight ( $M_{\rm n}$ ) and dispersity (D) were measured by a Viscotek gel permeation chromatography (GPC) instrument. The order-disorder transition temperature ( $T_{\rm ODT}$ ) of the SAS triblock copolymer was probed using a TA Instruments DHR-2 rheometer equipped with 25 mm parallel plates. The molecular characteristics of the SAS triblock copolymer used in this study are summarized in Table 1.

**Table 1:** Characteristics of the SAS triblock copolymer

M <sub>n</sub> of midblock (kg/mol)	57.3
M <sub>n</sub> of triblock copolymer (kg/mol)	76.2
Ð	1.67
vol% of styrene in triblock copolymer	23%
Todt (°C)	220.8

# **Rheological Measurements**

Ex situ rheological measurements were performed on a strain-controlled rheometer (ARES-G2, TA Instruments) equipped with a cone and partitioned plate geometry (25 mm outer diameter, 10 mm inner diameter and 0.1 rad cone angle). Sample disks with 25 mm diameter and 1 mm thickness were prepared by compression molding on a Carver hot press at an applied load of 4,200 lbs at 230 °C. Two different types of rheological tests were performed at 130 °C: (1) dynamic strain sweeps with strain amplitude ranging from 1 – 1000% were performed at frequencies of 1 and 10 rad/s and (2) dynamic time sweeps at a frequency of 10 rad/s were performed at strain amplitudes of 50, 100 and 150%.

Measurements were carried out using transient data collection mode, which records stress and strain wave-form data. The data were sampled with a density of 128 points/cycle. For dynamic strain sweeps, 20 cycles of oscillation were performed at each strain amplitude value to generate equilibrated oscillatory shear flow and only the last four cycles were analyzed. For dynamic time sweeps, the stress and strain wave-form data were collected continuously for the first 500 cycles. After that, 4 cycles of oscillation were collected for every 20 cycles. The stress and strain wave-form data were analyzed with "MITlaos" software.<sup>87</sup> The storage (G') and loss (G") moduli (from the primary frequency), third-order harmonic ( $I_{3/1}$ ), and third-order viscous ( $v_{3/V1}$ ) and elastic ( $e_{3/e_1}$ ) Chebyshev coefficients<sup>88</sup> were extracted.

### In Situ SAXS Measurements

Small-angle X-ray scattering experiments were performed at beamline 5ID-D at the Advanced Photon Source, Argonne National Laboratory with energy of 17 keV (corresponding to an X-ray wavelength of 0.7293 Å). Two-dimensional (2D) scattering patterns were collected at a

pixel resolution of  $1920 \times 1920$  pixels using a CCD detector at a sample to detector distance of 8.5 m.

A Linkam CSS-450 shear cell was installed on the beamline for shearing samples *in situ*. The sample disks (19 mm diameter and 1.6 mm thickness) for SAXS measurements were prepared by compression molding on a Carver hot press at an applied load of 4,200 lbs at 230 °C. Samples were placed between two preheated parallel pates covered with kapton tape (Figure 1). The shear cell was mounted such that the X-ray beam direction was perpendicular to the 1-3 plane of flow (e.g. the beam was oriented along the shear gradient ( $\vec{2}$ ) direction). The samples were sheared at a frequency of 10 rad/s with different strain amplitudes (50, 100 and 150%). SAXS data were collected using following protocols: (1) for strain amplitudes of 100 and 150%, data were collected at a rate of 1 frame/2 seconds with exposure time of 0.628 seconds for the first 3 min, then data collection was slowed down to 1 frame/6 seconds with exposure time of 0.2 second for 40 min. (2) For a strain amplitude of 50%, the data were collected at a rate of 1 frame/6 seconds with exposure time of 0.628 second for the first 30 min, then the data collection was slowed down to 1 frame/12 seconds with exposure time of 0.2 second for 40 min.

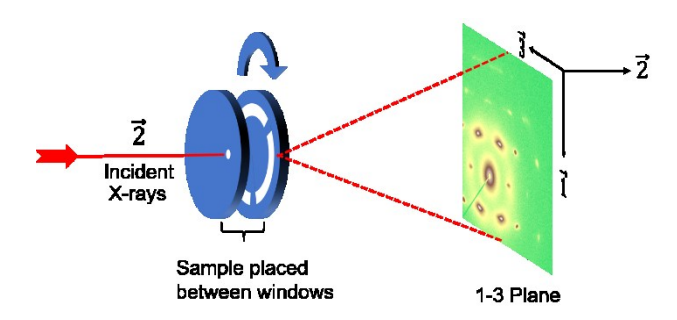


**Figure 1:** Schematic of shear cell mounted on the X-ray beamline, in which the X-ray beam is perpendicular to the 1-3 plane (and along the shear gradient direction). Coordinate axis indicates the velocity  $(\vec{1})$ , shear gradient  $(\vec{2})$ , and vorticity  $(\vec{3})$  directions.

# Results and Discussion

# **Disordered Spherical Morphology Observed Prior to Shearing**

The SAS triblock copolymer sample exhibited randomly oriented grains following compression molding, as evidenced by the isotropic ring in the 2D SAXS data (inset of Figure 2). The two-dimensional scattering pattern was azimuthally averaged to a one-dimensional profile of intensity versus scattering vector  $q = \frac{4\pi}{\lambda} \sin(\beta/2)$  ( $\beta$  is the scattering angle, and  $\lambda$  is the wavelength), shown in Figure 2. The 1D SAXS profile exhibited a sharp primary peak (q = 0.0277 Å<sup>-1</sup>) with weak higher order peaks, indicating microphase separation. The higher order peak locations were not consistent with traditional equilibrium bulk block copolymer phases (such as ordered lamellae, cylinders, body-centered cubic spheres, or a gyroid phase), but were characteristic of a disordered spherical morphology that has been previously reported by our group. To better understand the morphology, the 1D SAXS profile was fit with the Percus-Yevik hard sphere model (equation 1). The model assumes the presence of spherical polystryene domains (modeled as hard spheres) with average hard sphere radius  $R_{\rm sp}$ , radius of interaction  $R_{\rm hs}$  ( $R_{\rm hs} > R_{\rm sp}$ ) and effective volume fraction of hard spheres  $\eta$ :

$$I(q) = KN_s P(q)S(q) \tag{1}$$

where K is a constant that is a function of the type of radiation used and the sample properties,  $N_s$  is the number of scatters, P(q) is the spherical form factor (equation S1) and S(q) is the hard sphere structure factor with Percus–Yevick closure (equation S2).

The data fitting was performed using SasView, with combined functions of SphereModel and HardSphereStructure. The effect of size distribution of hard spheres was also incorporated into curve fitting by enabling the polydispersity function in SasView. The size distribution was characterized using  $PD=\sigma/R_{\rm sp}$ , where  $\sigma$  is the standard deviation. The SAXS data were well-

described with the Percus–Yevick model, revealing the disordered spherical morphology of SAS triblock copolymers. The parameters obtained from curve fitting were  $R_{sp} = 9$  nm,  $R_{hs} = 13$  nm,  $\eta = 0.55$  and PD = 0.14.

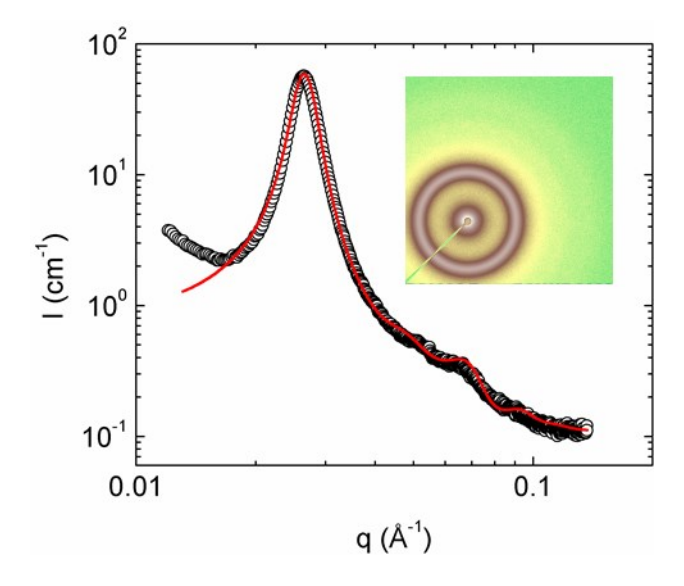


**Figure 2:** 1D SAXS profile obtained from the SAS triblock copolymer after compression molding (o) and Percus-Yevick hard-sphere model fit (red solid curve). Inset shows the 2D SAXS image.

# Nonlinear Viscoelastic Behavior of the SAS Triblock Copolymer

It is well known that the application of oscillatory shear in the nonlinear regime can induce microstructure alignment. The nonlinear regime can be identified by performing a strain sweep at a fixed frequency. In this study, a strain sweep was performed at 10 rad/s with strain amplitude  $\gamma$  = 1% – 1000%. The temperature was chosen as 130 °C, which is higher than the  $T_g$  of polystyrene (103 °C) and lower than the  $T_{\text{ODT}}$  of the SAS triblock copolymer (220 °C). Dynamic moduli (G' and G'') were plotted as a function of strain (Figure 3a). Two main regimes were observed in the G' and G'' behavior: the linear regime (also known as small-amplitude oscillatory shear (SAOS) regime) in which the dynamic moduli were independent of strain ( $\gamma$  = 1 – 10% in Figure 3a) and the nonlinear regime where the dynamic moduli decreased with strain, known as strain thinning ( $\gamma$  = 10 – 1000% in Figure 3a). Strain thinning behavior is typically observed in polymer solutions

and polymer melts, originating from chain orientation and alignment of microstructure along the flow direction that reduce the local viscous drag.<sup>90</sup>

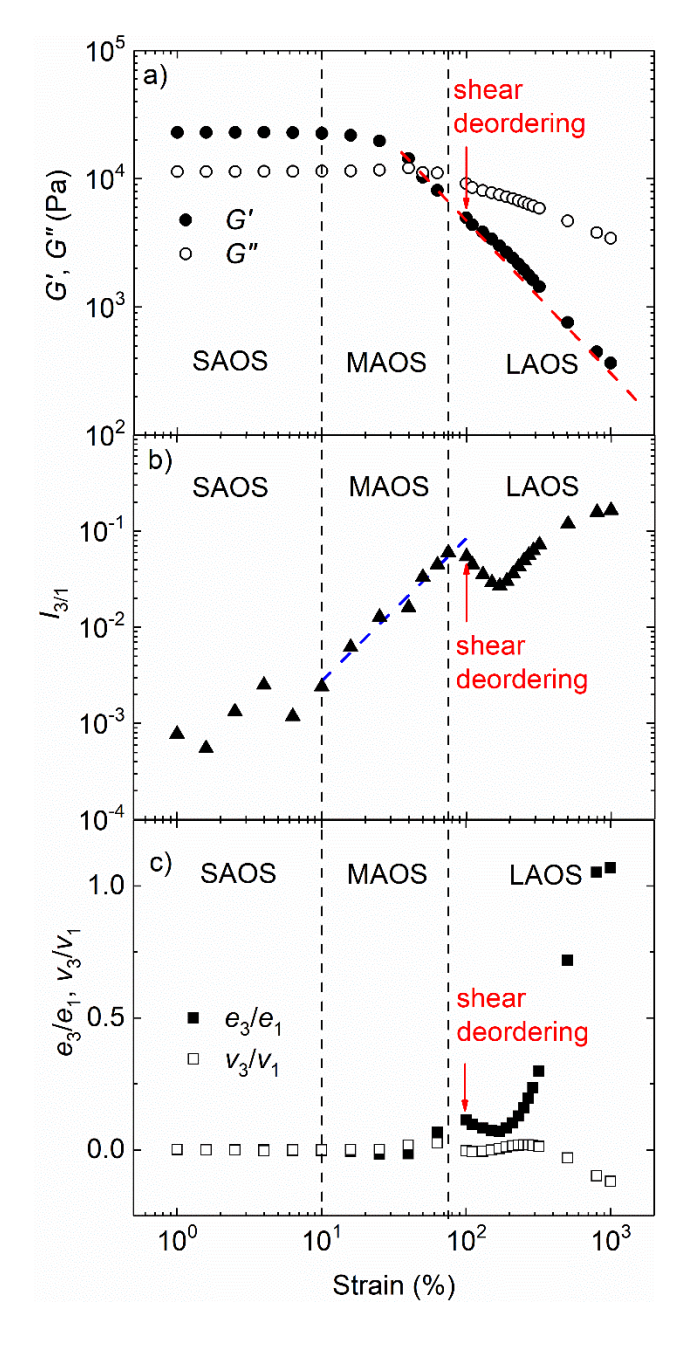


**Figure 3**: Oscillation strain sweeps of the SAS triblock copolymer at 130 °C and frequency of 10 rad/s: a) dynamic moduli, b) relative third harmonic,  $I_{3/1} = I_3/I_1$  and c) Chebyshev coefficients,  $e_3/e_1$  and  $v_3/v_1$ , as functions of strain  $\gamma$ . Red dashed line in a) is shown as a visual guide. Slope of blue dashed line in b) is 1.48.

Even though the dynamic moduli can provide useful information in the linear region, in the nonlinear regime where the higher order contributions become non-negligible analysis of the dynamic moduli alone is insufficient, as they only provide information on first order harmonic contributions. The higher order contributions can be quantified using Fourier transform (FT)rheology. FT-rheology converts stress data in the time domain (Figure 4 inset) to the frequency (\omega) domain (Figure 4), thus quantifying weak signals of the higher order harmonics. Among all the higher order harmonics, the relative intensity of the third order harmonic  $(I_{3/1} = I(3\omega)/I(\omega))$  has been proven to be powerful in quantifying the nonlinearity of materials.  $^{90,\,91}$  Figure 3b shows  $I_{3/1}$ as a function of strain. Based on different characteristics of  $I_{3/1}(\gamma)$ , the nonlinear region can be subdivided into two regimes: medium-amplitude oscillatory shear (MAOS) and large-amplitude oscillatory shear (LAOS) regimes. MAOS is an intermediate regime between SAOS and LAOS, characterized by a slope of two in the log-log plot of  $I_{3/1}$  vs  $\gamma$  for simple linear entangled polymer melts, and a slope of less than two in other cases such as presence of branching or strain hardening. 92 In our triblock copolymer, the slope was 1.48 in this regime ( $\gamma = 10\%$ -75% in Figure 3b). Interestingly, in the LAOS regime, a subregime was observed where  $I_{3/1}$  decreased with strain starting at  $\gamma = 100\%$ , corresponding to a shoulder in  $G'(\gamma)$ . This behavior is in contrast to most of the literature, in which  $I_{3/1}(\gamma)$  was sigmoidal. <sup>83, 90, 92</sup> Non-sigmoidal behavior has been reported for a block copolymer solution<sup>93</sup> and carbon black filled rubber<sup>94</sup>. López-Barrón et al observed a decrease of  $I_{3/1}$  in a block copolymer solution at high strain amplitude. 93 They ascribed the nonsigmoidal behavior to shear melting of hexagonally close-packed spheres at high strain amplitude, as observed in SANS measurements. Leblanc et al observed a "bump" in the intermediate strain amplitude due to strong interactions between a viscoelastic matrix (rubber) and a dispersed phase

(carbon black).<sup>94</sup> We ascribe the drop of  $I_{3/1}$  at  $\gamma$ =100-180% in Figure 3b to shear deordering that will be discussed in detail in the analysis of time-resolved SAXS data later in this manuscript.

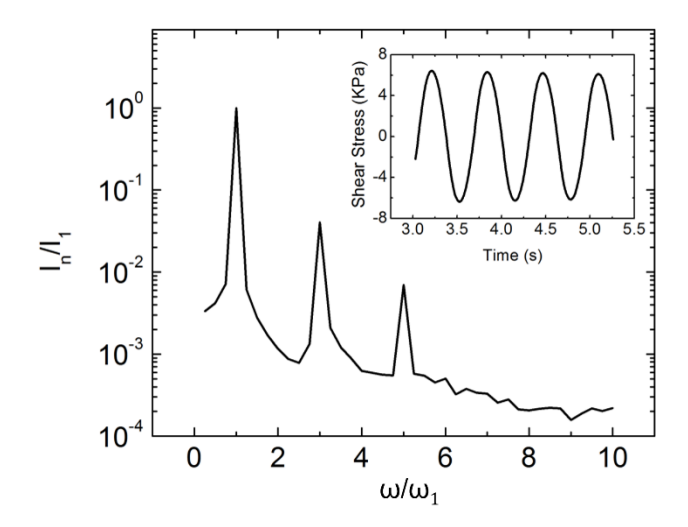


**Figure 4:** FT spectrum calculated from the time-dependent shear stress (from  $5^{th}$  to  $8^{th}$  oscillation cycles) of the SAS triblock copolymer under MAOS ( $\omega = 10 \text{ rad/s}$ ,  $\gamma = 50\%$ , T = 130 °C).

An alternative way to quantify nonlinearity is to use the relative third-order elastic and viscous Chebyshev coefficients ( $e_3/e_1$  and  $v_3/v_1$ , respectively). Ewoldt *et al* proposed stress decomposition using a set of orthogonal Chebyshev polynomials of the first kind, as defined in equations 2 and 3:

$$\sigma'(\bar{x}) = \gamma_0 \sum_{n=\text{odd}} e_n(\omega, \gamma_0) T_n(\bar{x})$$
(2)

$$\sigma''(\bar{y}) = \gamma_0 \sum_{\text{n=odd}} v_n(\omega, \gamma_0) T_n(\bar{y})$$
(3)

where  $\sigma'$  and  $\sigma''$  are the elastic and viscous stresses,  $\gamma_0$  is the maximum strain,  $e_n$  and  $v_n$  are the *n*th-order elastic and viscous Chebyshev coefficients,  $T_n(x)$  is the *n*th-order Chebyshev polynomial of the first kind, and  $\bar{x} = \gamma/\gamma_0$  and  $\bar{y} = \dot{\gamma}/\dot{\gamma}_0$  are the normalized instantaneous strain

and strain rate that provide the appropriate domains of [-1, +1] for orthogonality. <sup>88</sup> The Chebyshev coefficients allow the interpretation of intracycle nonlinearity where  $e_3 > 0$  indicates intracycle strain stiffening and  $e_3 < 0$  represents strain softening. Similarly,  $v_3 > 0$  indicates intracycle shear thickening and  $v_3 < 0$  describes shear thinning.

Figure 3c shows the Chebyshev coefficients as function of strain. In the SAOS regime, both  $e_3/e_1$  and  $v_3/v_1$  were close to zero as expected. In the MAOS regime,  $v_3/v_1$  and  $e_3/e_1$  started to increase with strain, indicating the sample exhibited nonlinearities in both elastic and viscous responses. The positive signs of  $v_3$  and  $e_3$  suggest intracycle shear thickening and strain stiffening. In the LAOS regime, shear deordering started at  $\gamma = 100\%$ , as evidenced by decrease of both  $v_3/v_1$  and  $e_3/e_1$ , coinciding with a drop of  $I_{3/1}$  and a shoulder in G'. The decreased  $v_3/v_1$  and  $e_3/e_1$  suggests less contribution from strain hardening and shear thickening due to reduction of long-range order because of shear deordering. With increasing strain amplitude ( $\gamma > 180\%$ ),  $e_3/e_1$  increased sharply while  $v_3/v_1$  decreased to negative values, suggests a transition from shear thickening to shear thinning at high strain values.

# **Exploring Domain Alignment through Time-Resolved SAXS**

To study the effect of strain on the kinetic pathway of alignment, *in situ* synchrotron SAXS were performed to investigate the time-dependent morphological evolution of the SAS triblock copolymer under varying strain amplitude with fixed frequency ( $\omega = 10 \text{ rad/s}$ ) at 130 °C. Three strain amplitudes were chosen, in different shear regimes, based on the results of the strain sweep:  $\gamma = 50\%$  in the MAOS regime,  $\gamma = 100\%$  in the LAOS regime and  $\gamma = 150\%$  in the shear deordering subregime of the LAOS regime. The structural evolution was monitored over the course of 40 and 140 min for strain amplitudes in LAOS and MAOS regimes, respectively. We note that our prior work utilizing *ex situ* SAXS measurements, in which data were taken in all three shear directions

(shear gradient  $(\vec{2})$ , velocity  $(\vec{1})$ , and vorticity  $(\vec{3})$  directions), established the presence of CP spheres (2D hexagonally close-packed (HCP) sphere layers arranged in co-existing 3D face-centered cubic (FCC) and HCP sphere morphologies) in this SAS triblock copolymer under shear alignment.<sup>78</sup> Here, we discuss *in situ* SAXS data obtained in the shear gradient direction  $(\vec{2})$  only,

Representative 2D SAXS data for the SAS triblock copolymer, obtained in the shear gradient  $(\vec{2})$  direction, under varying strain and different time stamps are shown in Figure 5. In the initial state (t = 0 s), the ring-like pattern in the 2D SAXS image indicates a macroscopically isotropic morphology with randomly oriented domains, as discussed previously. Upon application of oscillatory shear in the nonlinear regime, diffraction spots appeared and became sharp and bright under extended shearing, indicating the formation of macroscopically-aligned morphologies. The kinetics of alignment in the LAOS regime were significantly faster than that of the MAOS regime, evidenced by the fact that well-defined diffraction spots were fully developed within 90 s in the LAOS regime whereas in the MAOS regime the structures were not fully developed until after 40 min of oscillatory shear. The six spot pattern in the innermost ring is consistent with the presence of HCP layers (e.g. the (1 1 1) plane in the FCC structure or (0 0 0 1) plane in the HCP structure), 95 which was corroborated by ex situ SAXS data obtained in all three shear directions in our prior study. 78 The formation of HCP layers in HCP and/or FCC morphologies is also consistent with the observed shear thinning behavior (Figure 3a) as HCP planes of spheres comply easily with flow. 93, 96, 97

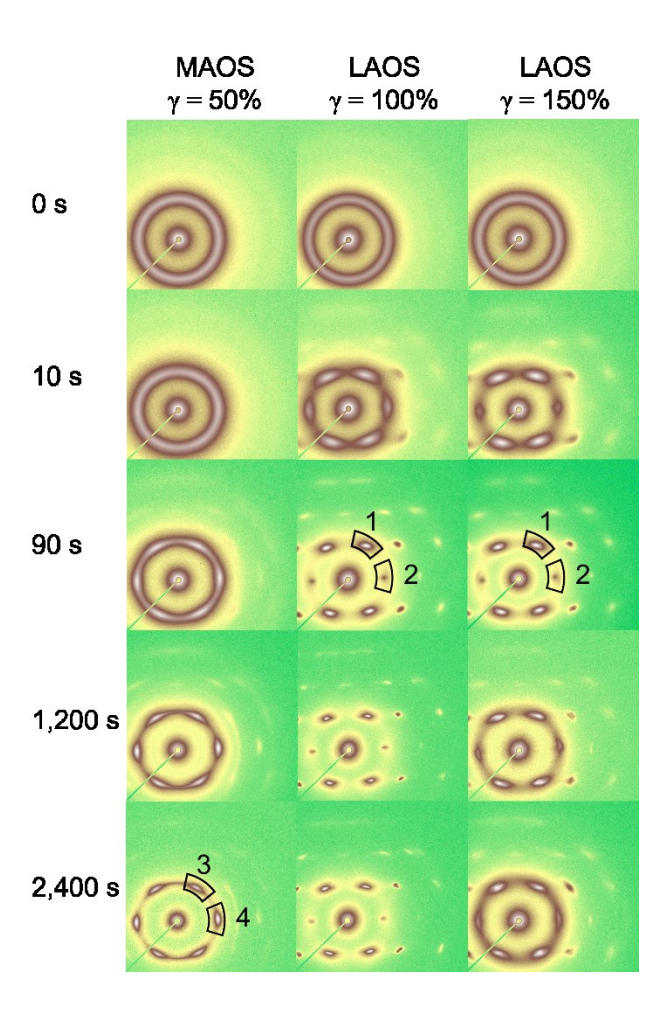


**Figure 5:** Representative 2D SAXS data obtained in the shear gradient direction  $(\overline{2})$ , with varying strain amplitudes ( $\gamma$ =50, 100 and 150%) at different time stamps (t=0, 10, 90, 1200 and 2400 s). Shear conditions used were  $\omega = 10$  rad/s and T = 130 °C. The following shear regimes have been identified for each condition: MAOS regime for  $\gamma = 50\%$ , LAOS regime for  $\gamma = 100\%$ , and shear deordering subregime of LAOS regime for  $\gamma = 150\%$ . At 90 s, non-equatorial and equatorial spots are highlighted as 1 and 2, respectively.

It is worth noting that in the LAOS regime ( $\gamma = 100$  and 150%), the two equatorial diffraction spots were less intense than the other four spots after alignment (*e.g.*, compare spots 1 and 2 at 90 s in Figure 5, which are non-equatorial and equatorial spots, respectively). Loose and Ackerson proposed a layer sliding mechanism indicating that HCP layers can slide over each other under shear using two types of motions: (i) under relatively low shear rates, the layers follow a zig-zag path and (ii) under relatively high shear rates, the layers follow a straight path parallel to the velocity direction ( $\vec{1}$ ). Theoretical calculations revealed that the zig-zag motion resulted in

partial reduction of the intensity of the two equatorial diffraction spots while the straight motion resulted in the disappearance of the two spots. The spot intensities in the equatorial and non-equatorial regions were monitored during alignment (Figures S1 and S2 for  $\gamma = 100$  and 150%, respectively). Whereas the non-equatorial spot showed little change in intensity over time, the equatorial spot intensity drastically decreased within the first 400 s before reaching a plateau. The equatorial and non-equatorial spots initially had similar intensities, and after alignment the equatorial spot intensity was reduced to around 10-20% of the non-equatorial spot intensity. Thus, we believe in the LAOS region, the HCP layers stacked along the shear gradient direction ( $\vec{2}$ ) (*i.e.*, the normal direction of the HCP layers was parallel to the shear gradient direction) and used a zigzag path to slide over one another.

Conversely, in the MAOS regime ( $\gamma = 50\%$ ), the two equatorial diffraction spots were brighter than the other four spots after alignment (Figure 5, compare spots 3 and 4 at t = 2,400 s). The spot intensities in the equatorial and non-equatorial regions were monitored during alignment (Figure S3). Initially, the intensities of equatorial and non-equatorial spots were similar, and with increasing alignment time the equatorial spot intensity increased while the non-equatorial spot intensity remained relatively constant. At 2,242 s, when anisotropic diffraction patterns became visible in the 2D SAXS data, both equatorial and non-equatorial spot intensities dropped drastically and then increased again. At longer alignment times, the equatorial spot intensity was around 2.2 times greater than that of the non-equatorial spot intensity. In contrast to the fully parallel orientation observed in the LAOS regime, we propose a biaxial orientation could be present in the MAOS regime. In a biaxial orientation, some of the HCP layers have a parallel orientation in which they are oriented parallel to the 1-3 plane (and perpendicular to the shear gradient direction ( $\vec{2}$ )), while other HCP layers have a perpendicular orientation in which they are

oriented parallel to the 1-2 plane (and perpendicular to the vorticity direction  $(\vec{3})$ ). This hypothesis is supported by comparing the 2D SAXS data with predicted Bragg peak positions (Figure 6a). The locations of Bragg peaks were calculated by inputting the space group symmetry, lattice constant and the direction of the beam following previously reported procedures.<sup>78</sup> In the perpendicular orientation, the norm of HCP layers is along the vorticity direction  $(\vec{3})$  (Figure 6b). In the parallel orientation, the norm of HCP layers is along the shear gradient direction  $(\vec{2})$ . The predicted Bragg peaks show good overlap with observed 2D SAXS data in Figure 6a in the primary ring of hexagonal spots. The appearance of the perpendicular orientation contributes to brighter intensity of the two equatorial spots. While the majority of literature studies on block copolymer solutions and melts demonstrated HCP layers with parallel orientation, <sup>93, 96, 98</sup> Daniel et al has reported the biaxial orientation of HCP layers for a block copolymer gel under steady shear flow at intermediate shear rates.<sup>74</sup> We do note, however, that not all predicted spots are observed in Figure 6 outside of the primary ring. This may be due to resolution limitations, as the concentration of spheres in the perpendicular orientation is likely much less than that in the parallel orientation, evidenced by the fact that the equatorial spot intensity was only slightly higher (factor of 2.2) than that of the non-equatorial spots. However, an alternative explanation for the diffraction pattern observed in Figure 6 is the stringing of spheres with long-range order along the  $\vec{1}$  direction, <sup>99</sup> which would also produce the higher equatorial spot intensity. The resolution of our data does not allow us to differentiate between these two possible explanations (e.g., biaxial orientation or stringing of spheres).

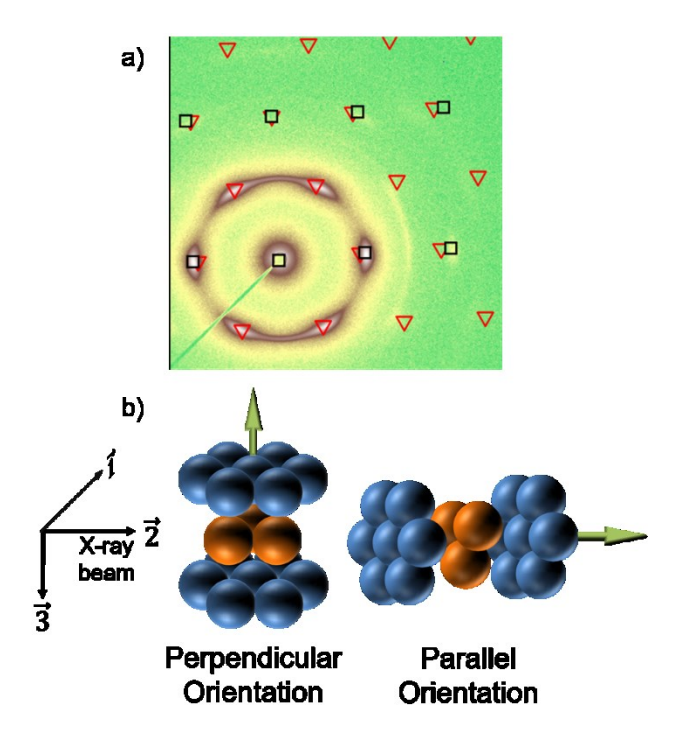


**Figure 6:** a) Comparison of 2D SAXS data obtained at  $\gamma = 50\%$  and t = 2,400 s with the predicted Bragg peaks for parallel (red  $\nabla$ ) and perpendicular (black  $\square$ ) orientations of HCP layers. b) Schematic of relative alignment of HCP layers with the shear axes. In the perpendicular orientation, the norm of HCP layers is along the vorticity direction ( $\vec{3}$ ), whereas in the parallel orientation, the norm of HCP layers is along the shear gradient direction ( $\vec{2}$ ). Here HCP layers with ABABAB stacking (A layers are blue and B layers are orange) are presented as an example.

#### **Kinetics of Shear Alignment**

To qualitatively study the alignment kinetics, the intensity as a function of azimuthal angle was determined for the innermost ring, and the anisotropic factor  $(A_f)$  was calculated to characterize the degree of alignment (equation 4):

$$A_f = \frac{\int_0^{2\pi} I(q^*, \theta) \cos[6(\theta - \theta_0)] d\theta}{\int_0^{2\pi} I(q^*, \theta) d\theta}$$
(4)

where  $q^*$  is the magnitude of the scattering vector of the innermost ring,  $\theta$  is the azimuthal angle, and the factor of 6 accounts for six-fold symmetry.<sup>51, 54, 78</sup>  $A_f$  ranges from 0 (fully isotropic) to 1 (fully aligned).  $A_f$  values are shown in Figure 7 as a function of shearing time. At early stages of

shearing (180 s for  $\gamma$  = 100 and 150%, and 1,800 s for  $\gamma$  = 50%), data were collected with exposure time 0.628 s, corresponding to one oscillation cycle, and thus the curves are smooth as the stroboscopic effects (intracycle melting and ordering) were smeared out. After that, the exposure time was reduced to 0.2 s, therefore the curves became noisy at longer times due to stroboscopic effects. 93, 100

In the MAOS regime ( $\gamma = 50\%$ ),  $A_f$  exhibited an initial steep increase and then slowly approached a plateau of  $A_f$ = 0.68. In the LAOS regime ( $\gamma$  = 100%) a more rapid increase of  $A_f$ was observed at short times as compared to in the MAOS regime, indicating faster orientation kinetics. In addition, the sample achieved a higher plateau  $A_f$  value ( $A_f = 0.75$  for  $\gamma = 100\%$ ), indicating greater degree of alignment in the LAOS regime. The plateau value of  $A_f$  remained constant at long times (neglecting the oscillations due to stroboscopic effects), indicating the formation of a stable macroscopic orientation despite the presence of continuing external mechanical excitation. At the highest strain amplitude ( $\gamma = 150\%$ ), also in the LAOS regime, instead of reaching a plateau, a maximum in  $A_f$  was observed at t = 180 s, after which  $A_f$  decreased over time. The decreasing  $A_f$  indicates the macroscopic orientation was not stable under continuing mechanical stimulus. The decreased degree of alignment is also evidenced by the strengthening of the intensity of the innermost isotropic ring at t = 1,200 s and 2,400 s (Figure 5), indicating partial melting of HCP layers. Recalling that  $I_{3/1}$  decreased with strain starting at  $\gamma = 100\%$  (Figure 3b), and  $G'(\gamma)$  exhibited a shoulder in the same strain region (Figure 3a), we propose this behavior is related to shear deordering. The observation of shear deordering at high strain amplitude indicates that macroscopic ordering under oscillatory shear is a complex process, and the degree of alignment is not only affected by the shear conditions (frequency, strain amplitude, temperature), but also by the duration of applied shear.

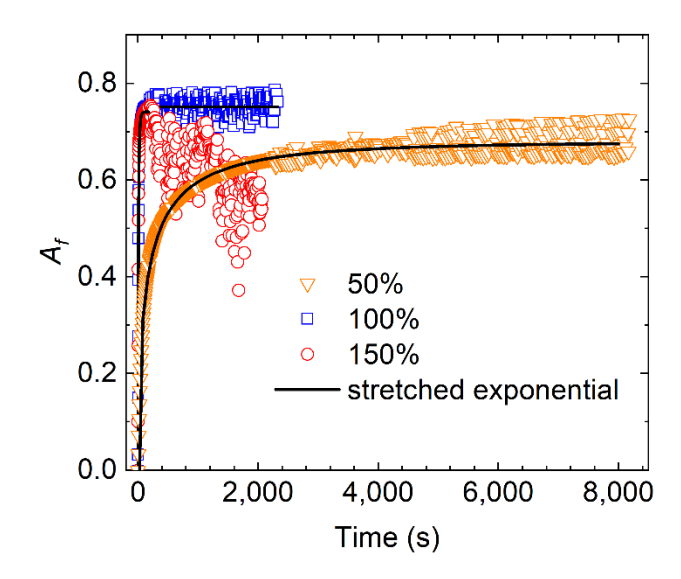


**Figure 7:** Anisotropic factor  $(A_f)$  as function of shearing time for  $\gamma = 50\%$  (orange  $\nabla$ ), 100% (blue  $\square$ ) and 150% (red  $\circ$ ). The solid lines are stretched exponential fitting (eqn. 5).

Only a few studies have reported the presence of shear deordering. A concentrated diblock copolymer solution exhibited shear deordering under reciprocating shear field with high frequency, in which well-defined perpendicular lamellae transitioned to a poorly defined parallel orientation under continuous mechanical stimulus. A diblock copolymer melt under LAOS with high strain amplitudes exhibited shear ordering in which perpendicular lamellae transitioned to a biaxial orientation under further application of shear. Shear melting has also been reported in BCC block copolymer melts under unidirectional shear. To the best of our knowledge, we are the first to report on the shear deordering of a bulk block copolymer with CP spherical morphology.

To quantitatively study the kinetics of shear alignment, the time dependence of  $A_f$  was fit with a stretched exponential function (equation 5). The stretched exponential function was modified to conform to the following boundary conditions: when t = 0,  $A_f = 0$  and when  $t = \infty$ ,  $A_f = A_{f,0}$ :

$$A_f = A_{f,0} (1 - e^{-(t/\tau)^{\beta}}) \tag{5}$$

where  $A_{f,0}$  is the plateau value,  $\tau$  is the characteristic alignment time and  $\beta$  is the "heterogeneity index" that represents the width of the alignment time distribution. The stretched exponential function has been widely used to describe the time-dependent shear-induced alignment processes.<sup>38, 82, 103</sup> Disordered polymer melts possess a heterogeneous distribution of grain sizes, shapes and orientations, and thus a broad distribution of orientation times  $\tau$  are usually observed, resulting in deviation from the ideal single exponential function ( $\beta = 1$ ). The fitted exponential function curves are shown in Figure 7 as solid curves and fitting results are tabulated in Table 1. Note that for  $\gamma = 150\%$ , only the data for the first 180 s were fit (before the onset of shear deordering).

**Table 1:** Parameters extracted from fitting the stretched exponential function (equations 5, 6, and 7) to the time-dependent  $A_f$ , normalized moduli (G', G'') and  $I_{3/1}$  at various  $\gamma$ 

$A_f$				
γ	$A_{f,0}$	τ (s)	β	
50%	$0.678 \pm 0.002$	210 ± 5	$0.42 \pm 0.05$	
100%	$0.751 \pm 0.002$	$10.4 \pm 0.5$	$0.67 \pm 0.08$	
150%	$0.741\pm0.004$	$7.2 \pm 0.6$	$0.75 \pm 0.08$	
Normalized $G'$				
γ	$G_0^\prime$ a	$\tau(s)$	β	
50%	$0.536 \pm 0.002$	25 ± 1	$0.38 \pm 0.02$	
100%	$0.818 \pm 0.002$	$9\pm1$	$0.80 \pm 0.08$	
150%	$0.902 \pm 0.001$	8 ± 1	$0.86 \pm 0.08$	
	Normalized G"			
γ	$G_0^{"}$ a	$\tau(s)$	β	
50%	$0.670 \pm 0.003$	56 ± 2	$0.35 \pm 0.02$	
100%	$0.844\pm0.002$	$8 \pm 1$	$0.85 \pm 0.09$	
150%	$0.907 \pm 0.003$	5 ± 1	$0.95\pm0.05$	
	$I_{3/1}$			
γ	$I_{3/1,0}$	$\tau(s)$	β	
50%	$-0.135 \pm 0.005$	43 ± 3	$0.25\pm0.02$	
100%	$0.025\pm0.001$	$31 \pm 2$	$0.7 \pm 0.1$	
150%	$0.026\pm0.001$	$16 \pm 2$	$0.71 \pm 0.08$	

 $<sup>^{\</sup>mathrm{a}}\,G_0'$  and  $G_0^{''}$  are unitless as eqn. 6 describes the normalized G' and G''

As expected,  $A_{f,0}$  increased with strain amplitude while  $\tau$  decreased, indicating larger deformation produced higher degree of alignment and faster kinetics. The orientation time  $\tau$  exhibited a broad distribution ( $\beta$  < 1), and  $\beta$  increased with strain amplitude, indicating defects (e.g., heterogeneity in grain size, shape, orientation) were effectively removed by applying larger deformation. The increase in  $A_{f,0}$ , decrease in  $\tau$ , and increase in  $\beta$  with increasing strain amplitude are consistent with a prior literature study on a lamellae-forming block copolymer.<sup>82</sup>

# **Correlation of Morphological Changes and Mechanical Response**

To correlate morphological properties (e.g., degree of alignment, grain orientation) with rheological properties (e.g., moduli, nonlinearity), orientation of the SAS triblock copolymer was explored using a rheometer with cone partitioned-plate geometry, under the same shear conditions employed in the SAXS experiments (T = 130 °C,  $\omega$  = 10 rad/s,  $\gamma$  = 50, 100 and 150%). Both storage and loss moduli were normalized by their maximum value (normalized  $G' = G'/G'_{max}$ , normalized  $G'' = G''/G''_{max}$ ) in order to qualitatively compare the time progression of moduli under different strain amplitudes (Figure 8). Under all shear conditions, both storage and loss moduli exhibited an initial sharp decrease due to the removal of defects and the formation of HCP layers that comply easily with flow, similar to that observed in  $A_f$  in Figure 7. For  $\gamma = 50$  and 100%, the moduli reached plateau values indicating stable structures were formed, consistent with morphological observations under SAXS. By contrast, at  $\gamma = 150\%$  the moduli reached a minimum value at short time then increased upon continuous shearing. Recall that Afguantified from in situ SAXS reached a maximum value and then decreased with further shearing time, indicating shear-induced deordering Similarly, we attribute the increase of the moduli at long shearing times to the increased number of defects as a result of shear deordering.

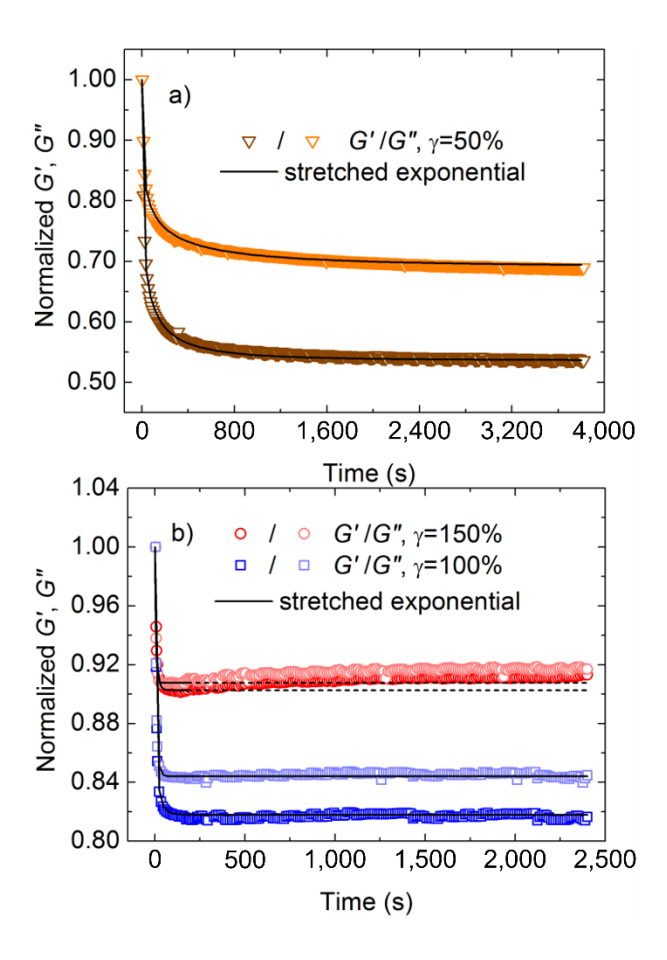


**Figure 8:** Normalized moduli (G' and G'') as a function of time for the a) MAOS regime ( $\gamma = 50\%$ ) and b) LAOS regime ( $\gamma = 100\%$  and 150%). The solid curves are stretched exponential fits to the data (equation 6). The dashed horizontal lines are included as visual guides.

The time progression of the normalized storage modulus under various strain amplitudes was modeled with a stretched exponential function (equation 6):

Normalized 
$$G' = (1 - G'_0) \left( e^{-\left(\frac{t}{\overline{\tau}}\right)^{\beta}} - 1 \right) + 1$$
 (6)

where  $G'_0$  is the plateau value. An analogous equation was applied to the time progression of normalized G'', with  $G''_0$  as the plateau value. The results of fitting equation 6 to the data are shown as solid curves in Figure 8. Note that for  $\gamma = 150\%$ , only the data during the first 180 s were used for fitting (prior to onset of shear deordering). The extracted fit parameters are tabulated in Table 1. The observed trends are quantitatively similar to that discussed for the time progression of  $A_f$ .

Comparable analyses were also conducted without normalization of the moduli, which yielded very similar values of  $\tau$  and  $\beta$  (Figure S4 and Table S1).

However, the normalized moduli do not provide much information as the stress curves become distorted under MAOS and LAOS flow. We therefore examined the nonlinear stress data using the ideas developed in FT-rheology. The relative intensity of the third harmonic ( $I_{3/1}$ ) was chosen to monitor the alignment process. Previous studies have shown that  $I_{3/1}$  is sensitive to microstructural changes, and thus it is suitable to assess macroscopic orientation.<sup>38, 82, 85, 103</sup> Two completely different behaviors were observed in  $I_{3/1}$  in the MAOS and LAOS regimes (Figure 9): in the MAOS region,  $I_{3/1}$  increased upon shearing, while in the LAOS region,  $I_{3/1}$  decreased upon shearing. Generally,  $I_{3/1}$  is proportional to the number of defects.<sup>38, 82</sup> Under shear flow, the grain interfaces (defects) undergo deformations that give rise to the nonlinear stress response. Typically, during the shear alignment process, the number of defects is anticipated to decrease as the microdomains become more oriented, thus decreasing  $I_{3/1}$ . This rationale explains the observation in the LAOS region that  $I_{3/1}$  decreased upon shearing.

It is quite unusual that  $I_{3/1}$  increased with time in the MAOS region. An increase of  $I_{3/1}$  with application of shear has been reported previously for block copolymer lamellae, upon reorientation from parallel to perpendicular orientations.<sup>38</sup>It has also been reported for the orientation of liquid crystals under oscillatory shear, in which poor orientation was observed at relatively small strain amplitude (in the nonlinear regime), and shear flow did not result in well-oriented lamellae.<sup>103</sup> Thus, differently oriented grains showed different stress levels, especially at grain boundaries, which resulted in more distorted macroscopic stress curves. In Figure 9 in the MAOS regime,  $I_{3/1}$  increased sharply and then reached a plateau. We previously identified the presence of coexisting parallel and perpendicular orientations of HCP layers (*e.g.*, discussion on Figure 6). Thus, we

hypothesize that upon shearing, some of the parallel HCP layers reoriented to the perpendicular direction, resulting in increased number of defects (boundary between grains) and therefore larger  $I_{3/1}$ .

The time progressions of  $I_{3/1}$  under various strain amplitudes were also modeled with the stretched exponential function (equation 7):

$$I_{3/1} = I_{3/1.0} e^{-\left(\frac{t}{\tau}\right)^{\beta}} + C \tag{7}$$

where C is the plateau value (C = 0.1347, 0.03328, and 0.01476 for  $\gamma$  = 50, 100, and 150%, respectively). The fit of equation 7 to the data is shown as solid curves in Figure 9 and the resulting fit parameters tabulated in Table 1. A negative value of  $I_{3/1,0}$  is indicative of increase in  $I_{3/1}$  with time (e.g., observed at  $\gamma$  = 50%), while a positive value represents a decrease with time (e.g., observed at  $\gamma$  = 100 and 150%). Similar to the results obtained from fitting the stretched exponential to  $A_f$  and the normalized moduli, the characteristic ordering time decreased with increasing strain amplitude, indicating faster dynamics at higher strain amplitudes, and the heterogeneity index  $\beta$  increased with strain amplitude, indicating formation of a more homogeneous grain size distribution at higher strain amplitudes.

It is worth noting that the values of  $\tau$  and  $\beta$  are method-dependent and differing values are obtained when fitting the stretched exponential function to  $A_f$ , G', G" and  $I_{3/1}$ ; however, the qualitative trends observed in  $\tau$  and  $\beta$  with applied shear amplitude were consistent regardless of the measurement technique used.

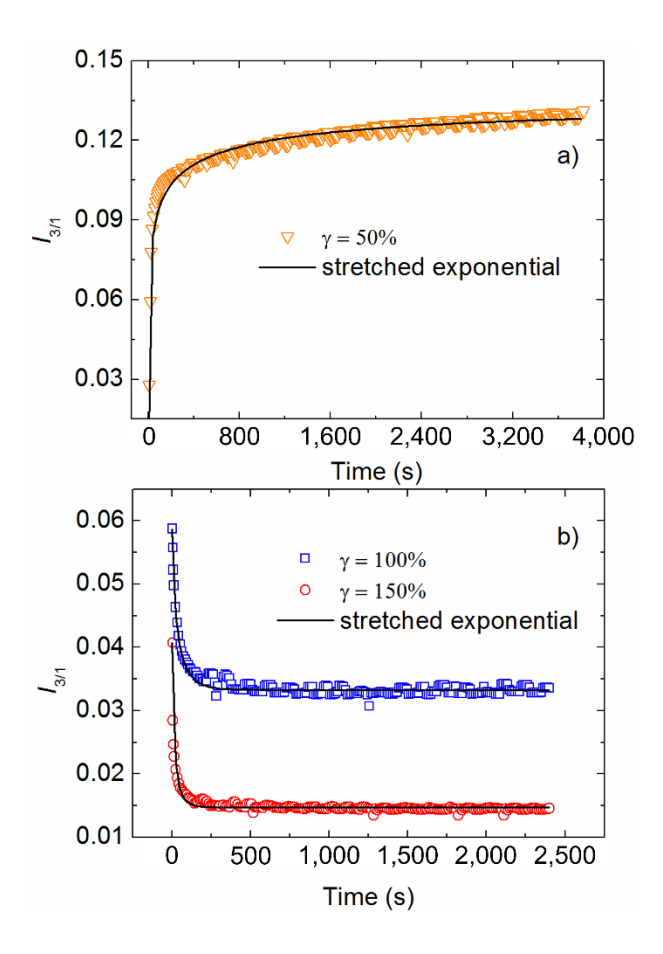


**Figure 9:** a) Time progression of  $I_{3/1}$  for the a) MAOS regime ( $\gamma = 50\%$ ) and b) LAOS regime ( $\gamma = 100$  and 150%). Solid curves are stretched exponential fits (equation 7) to the data.

## **Identification of Alignment Mechanism**

To understand the alignment mechanism, 2D SAXS data obtained at early stages (180 s for  $\gamma = 100$  and 150%, and 1,800 s for  $\gamma = 50\%$ ) were azimuthally averaged and compared to one another (Figures 10 and S5). Several noticeable changes in the 1D SAXS data were observed during the alignment process. First, the primary peak became sharper and shifted to lower q (e.g., from 0.0266 to 0.0255 Å<sup>-1</sup> at  $\gamma = 100\%$  in Figure 10), indicating structural rearrangement resulting in larger domain spacing and greater ordering. Second, the primary peak corresponding to the Percus-Yevick structure factor disappeared (shown by the black arrow in Figure 10) and new peaks appeared at q = 0.0425 and 0.0512 Å<sup>-1</sup> (corresponding to  $\sqrt{3}q^*$  and  $\sqrt{4}q^*$ , respectively) as the

alignment proceeded. Similar behavior was observed at all strains ( $\gamma = 50$ , 100 and 150%), with some distortion of hexagonal in-layer packing present at  $\gamma = 50\%$  (Figure S5).

Previous studies have proposed two types of alignment mechanisms: grain rotation and domain dissolution and reformation (or melting and recrystallization).  $^{10, 29, 51, 84, 104, 105}$  Grain rotation requires the initial sample to consist of grains with a well-aligned structure within each grain, but not aligned with respect to each other. Under shear, the grains remain intact and rotate as hard bodies until the preferred orientation is achieved. By contrast, in domain dissolution and reformation, domains with unfavorable orientation are first melted and then re-formed piece by piece to the preferred orientation to achieve a globally aligned structure. We propose that the SAS triblock copolymer has aligned through the domain dissolution and reformation mechanism. The dissolution of domains is confirmed by the disappearance of the Percus-Yevick structure factor peak, indicating melting of disordered spherical structures in the sample. Meanwhile, new domains with CP spherical structures were formed, as evidenced by the appearance of the new peaks at  $\sqrt{3}g^*$  and  $\sqrt{4}g^*$ .

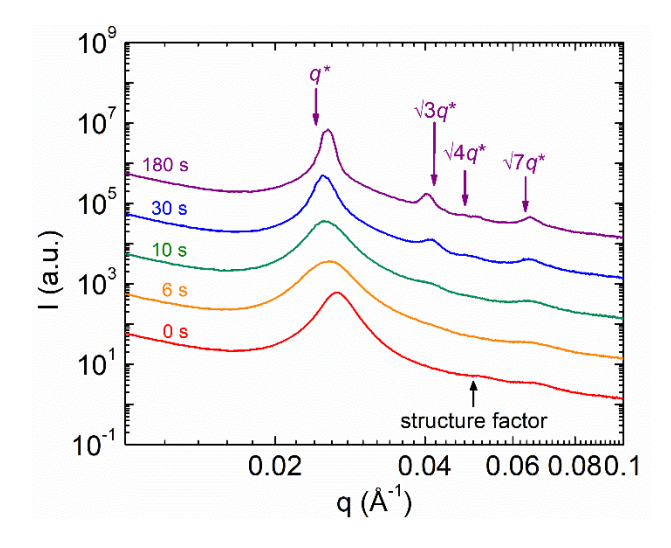


**Figure 10:** 1D azimuthally averaged SAXS profiles obtained at different times (0, 6, 10, 30 and 180 s) at strain  $\gamma = 100\%$ . Data are shifted by the following factors:  $10^0$  (0 s),  $10^1$  (6 s),  $10^2$  (10 s),  $10^3$  (30 s), and  $10^4$  (180 s). Purple arrows indicate locations of primary and secondary peak positions as expected for CP spheres based on the HCP unit cell with dimensions a/c = 0.66 and c

= 45.7 nm (theoretical peak locations were determined by fitting 2D SAXS data and calculating  $q^*$  from the resulting unit cell a and c values). Black arrow indicates location of primary peak associated with the Percus-Yevick structure factor for hard spheres. 1D SAXS profiles for  $\gamma = 50$  and 150% are shown in Figure S5.

#### Conclusions

The kinetics and mechanisms of alignment of poly(styrene-b-lauryl acrylate-b-styrene) triblock copolymers with an initially disordered spherical morphology were investigated. Disordered spheres transitioned to a close-packed (CP) spherical morphology under nonlinear oscillatory shear. Shear regimes were identified through FT-rheology. In the SAOS regime, G' and G'' were independent of  $\gamma$ , and  $I_{3/1}$ ,  $e_3/e_1$  and  $v_3/v_1$  were negligible. In the MAOS regime, G' decreased due to strain thinning,  $I_{3/1}$  vs.  $\gamma$  exhibited a slope of 2 on a log-log plot, and  $e_3/e_1$  and  $v_3/v_1$  started to increase due to intracycle shear thickening and strain stiffening. In the LAOS regime, both G' and G'' decreased due to strain thinning and shear deordering was observed through the presence of a shoulder in G' and decrease in  $I_{3/1}$ ,  $v_3/v_1$  and  $e_3/e_1$ . As  $\gamma$  further increased,  $I_{3/1}$  increased once again due to grain reformation, and  $e_3/e_1$  increased sharply while  $v_3/v_1$  decreased to negative values, suggests a transition from shear thickening to shear thinning at high strain values.

Time-dependent microstructural changes were evaluated using *in situ* SAXS. At fixed temperature (T = 130°) and frequency ( $\omega$  = 10 rad/s), increasing strain amplitude resulted in not only faster ordering but also a higher degree of orientation. Two types of orientations of HCP layers were observed: 1) parallel orientation of HCP layers in the LAOS region ( $\gamma$  = 100 and 150%) and 2) a more irregular biaxial or sphere stringing orientation in the MAOS regime (at  $\gamma$  = 50%). In the LAOS regime, the HCP layers stacked along the shear gradient direction and used a zig-zag path to slide over one another. Interestingly, for the first time, we observed shear deordering of CP spheres under oscillatory shear, observed at the highest strain amplitude ( $\gamma$  = 150%). At short times

(180 s), a highly ordered CP spherical morphology was achieved at  $\gamma = 150\%$ ; however, it degenerated to become less ordered upon extended shear. Structural rearrangements were consistent with the domain dissolution and reformation mechanism, in which the unfavorable disordered spheres first melted and then reformed in the preferred CP structure.

Mechanical responses were correlated to morphological changes. The anisotropic factor  $A_f$  sharply increased with increasing shear time, reaching a plateau value in MAOS and LAOS regimes.  $A_f$  was higher in the LAOS regime as compared to MAOS regime, and under shear deordering,  $A_f$  reached a maximum value and subsequently decreased with longer shearing times. For all shear conditions, both G' and G'' decreased significantly upon ordering due to formation of HCP layers that exhibited less resistance to flow. At  $\gamma = 150\%$ , the moduli initially decreased sharply followed by a slight increase, attributed to the shear deordering process observed with in situ SAXS. Two opposite behaviors of time-dependent changes of  $I_{3/1}$  were observed:  $I_{3/1}$  increased with time in the MAOS regime and decreased with time in the LAOS regime. The decrease of  $I_{3/1}$  in the LAOS region is anticipated during ordering due to continuous removal of defects and thus presence of fewer grain boundaries. The unexpected increase of  $I_{3/1}$  in the MAOS region is hypothesized to originate from the presence of sharp grain interphase boundaries (defects) due to the biaxial orientation or sphere stringing, that gave rise to increased  $I_{3/1}$ .

Changes in the anisotropic factor  $A_f$  quantified from *in situ* SAXS data, normalized moduli, and  $I_{3/1}$  with shearing time were modeling with stretched exponential functions. In all cases, the characteristic ordering time decreased with increasing strain amplitude, indicating faster dynamics at higher strain amplitudes, and the heterogeneity index  $\beta$  increased with strain amplitude, indicating formation of a more homogeneous grain size distribution at higher strain amplitudes.

# Acknowledgements

The authors thank Shu Wang for synthesis of the SAS triblock copolymers, and Tyler Cooksey and Minjie Shen for assisting with SAXS experiments. The authors thank Randy Ewoldt for providing the MITLAOS software for the FT-rheology analysis and Eric W. Cochran for providing the software for prediction of 2D SAXS diffraction patterns. This research used resources of the Advanced Photon Source, a U.S. Department of Energy (DOE) Office of Science User Facility operated for the DOE Office of Science by Argonne National Laboratory under Contract No. DE-AC02-06CH11357. This material is based upon work supported by the National Science Foundation under Grants No. DMR-1351788 and DMR-1906009.

# **Supporting Information**

The following supporting information is included: spherical form factor and Percus-Yevick structure factor (equations S1 and S2); quantification of equatorial and non-equatorial spot intensities over time (Figures S1-S3); stretched exponential fitting to non-normalized G' and G' (Figure S4 and Table S1); and 1D SAXS data analysis (Figure S5).

# References

- 1. Radjabian, M.; Abetz, V., Advanced porous polymer membranes from self-assembling block copolymers. *Progress in Polymer Science* **2020**, *102*.
- 2. Nian, S.; Lian, H.; Gong, Z.; Zhernenkov, M.; Qin, J.; Cai, L.-H., Molecular Architecture Directs Linear—Bottlebrush—Linear Triblock Copolymers to Self-Assemble to Soft Reprocessable Elastomers. *ACS Macro Letters* **2019**, *8* (11), 1528-1534.
- 3. Ding, Y.; Feng, W.; Huang, D.; Lu, B.; Wang, P.; Wang, G.; Ji, J., Compatibilization of immiscible PLA-based biodegradable polymer blends using amphiphilic di-block copolymers. *European Polymer Journal* **2019**, *118*, 45-52.
- 4. Jeong, S.-J.; Kim, J. Y.; Kim, B. H.; Moon, H.-S.; Kim, S. O., Directed self-assembly of block copolymers for next generation nanolithography. *Materials Today* **2013**, *16* (12), 468-476.
- 5. Black, C. T.; Ruiz, R.; Breyta, G.; Cheng, J. Y.; Colburn, M. E.; Guarini, K. W.; Kim, H.-C.; Zhang, Y., Polymer self assembly in semiconductor microelectronics. *IBM Journal of Research and Development* **2007**, *51* (5), 605-633.
- 6. Chan, V. Z.-H.; Hoffman, J.; Lee, V. Y.; Iatrou, H.; Avgeropoulos, A.; Hadjichristidis, N.; Miller, R. D.; Thomas, E. L., Ordered Bicontinuous Nanoporous and Nanorelief Ceramic Films from Self Assembling Polymer Precursors. *Science* **1999**, *286* (5445), 1716-1719.
- 7. Ma, W.; Yang, C.; Gong, X.; Lee, K.; Heeger, A. J., Thermally Stable, Efficient Polymer Solar Cells with Nanoscale Control of the Interpenetrating Network Morphology. *Advanced Functional Materials* **2005**, *15* (10), 1617-1622.
- 8. Guo, C.; Lin, Y.-H.; Witman, M. D.; Smith, K. A.; Wang, C.; Hexemer, A.; Strzalka, J.; Gomez, E. D.; Verduzco, R., Conjugated Block Copolymer Photovoltaics with near 3% Efficiency through Microphase Separation. *Nano Letters* **2013**, *13* (6), 2957-2963.
- 9. Borges, B. G. A. L.; Veiga, A. G.; Tzounis, L.; Laskarakis, A.; Logothetidis, S.; Rocco, M. L. M., Molecular Orientation and Ultrafast Charge Transfer Dynamics Studies on the P3HT:PCBM Blend. *The Journal of Physical Chemistry C* **2016**, *120* (43), 25078-25082.
- 10. Chen, Z.-R.; Kornfield, J. A., Flow-induced alignment of lamellar block copolymer melts. *Polymer* **1998,** *39* (19), 4679-4699.
- 11. Hermel, T. J.; Wu, L.; Hahn, S. F.; Lodge, T. P.; Bates, F. S., Shear-Induced Lamellae Alignment in Matched Triblock and Pentablock Copolymers. *Macromolecules* **2002**, *35* (12), 4685-4689.
- 12. Stangler, S.; Abetz, V., Orientation behavior of AB and ABC block copolymers under large amplitude oscillatory shear flow. *Rheologica Acta* **2003**, *42* (6), 569-577.
- 13. Olszowka, V.; Hund, M.; Kuntermann, V.; Scherdel, S.; Tsarkova, L.; Böker, A., Electric Field Alignment of a Block Copolymer Nanopattern: Direct Observation of the Microscopic Mechanism. *ACS Nano* **2009**, *3* (5), 1091-1096.
- 14. Liedel, C.; Pester, C. W.; Ruppel, M.; Lewin, C.; Pavan, M. J.; Urban, V. S.; Shenhar, R.; Bösecke, P.; Böker, A., Block Copolymer Nanocomposites in Electric Fields: Kinetics of Alignment. *ACS Macro Letters* **2013**, *2* (1), 53-58.
- 15. Hammond, M. R.; Dietsch, H.; Pravaz, O.; Schurtenberger, P., Mutual Alignment of Block Copolymer–Magnetic Nanoparticle Composites in a Magnetic Field. *Macromolecules* **2010**, *43* (20), 8340-8343.
- 16. Gopinadhan, M.; Choo, Y.; Kawabata, K.; Kaufman, G.; Feng, X.; Di, X.; Rokhlenko, Y.; Mahajan, L. H.; Ndaya, D.; Kasi, R. M.; Osuji, C. O., Controlling orientational order in block copolymers using low-intensity magnetic fields. *Proceedings of the National Academy of Sciences* **2017**, *114* (45), E9437-E9444.

- 17. Hashimoto, T.; Bodycomb, J.; Funaki, Y.; Kimishima, K., The Effect of Temperature Gradient on the Microdomain Orientation of Diblock Copolymers Undergoing an Order–Disorder Transition. *Macromolecules* **1999**, *32* (3), 952-954.
- 18. Singh, G.; Yager, K. G.; Smilgies, D.-M.; Kulkarni, M. M.; Bucknall, D. G.; Karim, A., Tuning Molecular Relaxation for Vertical Orientation in Cylindrical Block Copolymer Films via Sharp Dynamic Zone Annealing. *Macromolecules* **2012**, *45* (17), 7107-7117.
- 19. Singh, G.; Yager, K. G.; Berry, B.; Kim, H.-C.; Karim, A., Dynamic Thermal Field-Induced Gradient Soft-Shear for Highly Oriented Block Copolymer Thin Films. *ACS Nano* **2012**, *6* (11), 10335-10342.
- 20. Kim, S. H.; Misner, M. J.; Xu, T.; Kimura, M.; Russell, T. P., Highly Oriented and Ordered Arrays from Block Copolymers via Solvent Evaporation. *Advanced Materials* **2004**, *16* (3), 226-231.
- 21. Park, S.; Wang, J.-Y.; Kim, B.; Chen, W.; Russell, T. P., Solvent-Induced Transition from Micelles in Solution to Cylindrical Microdomains in Diblock Copolymer Thin Films. *Macromolecules* **2007**, *40* (25), 9059-9063.
- 22. Albert, J. N. L.; Young, W.-S.; Lewis, R. L.; Bogart, T. D.; Smith, J. R.; Epps, T. H., Systematic Study on the Effect of Solvent Removal Rate on the Morphology of Solvent Vapor Annealed ABA Triblock Copolymer Thin Films. *ACS Nano* **2012**, *6* (1), 459-466.
- 23. Segalman, R. A.; Yokoyama, H.; Kramer, E. J., Graphoepitaxy of Spherical Domain Block Copolymer Films. *Advanced Materials* **2001**, *13* (15), 1152-1155.
- 24. Cheng, J. Y.; Ross, C. A.; Thomas, E. L.; Smith, H. I.; Vancso, G. J., Fabrication of nanostructures with long-range order using block copolymer lithography. *Applied Physics Letters* **2002**, *81* (19), 3657-3659.
- 25. Cheng, J. Y.; Zhang, F.; Chuang, V. P.; Mayes, A. M.; Ross, C. A., Self-Assembled One-Dimensional Nanostructure Arrays. *Nano Letters* **2006**, *6* (9), 2099-2103.
- 26. Shin, G.; Sakamoto, N.; Saijo, K.; Suehiro, S.; Hashimoto, T.; Ito, K.; Amemiya, Y., Time-resolved SAXS studies of a sphere-forming block copolymer under large oscillatory shear deformation. *Macromolecules* **2000**, *33* (24), 9002-9014.
- 27. Huang, Y.-Y.; Hsu, J.-Y.; Chen, H.-L.; Hashimoto, T., Existence of fcc-Packed Spherical Micelles in Diblock Copolymer Melt. *Macromolecules* **2007**, *40* (3), 406-409.
- 28. Lee, S.; Bluemle, M. J.; Bates, F. S., Discovery of a Frank-Kasper σ Phase in Sphere-Forming Block Copolymer Melts. *Science* **2010**, *330* (6002), 349-353.
- 29. Morrison, F. A.; Winter, H. H., The effect of unidirectional shear on the structure of triblock copolymers. I. Polystyrene-polybutadiene-polystyrene. *Macromolecules* **1989**, *22* (9), 3533-3540.
- 30. Pakula, T.; Saijo, K.; Kawai, H.; Hashimoto, T., Deformation behavior of styrene-butadiene-styrene triblock copolymer with cylindrical morphology. *Macromolecules* **1985**, *18* (6), 1294-1302.
- 31. Osuji, C.; Zhang, Y.; Mao, G.; Ober, C. K.; Thomas, E. L., Transverse Cylindrical Microdomain Orientation in an LC Diblock Copolymer under Oscillatory Shear. *Macromolecules* **1999**, *32* (22), 7703-7706.
- 32. Vigild, M. E.; Almdal, K.; Mortensen, K.; Hamley, I. W.; Fairclough, J. P. A.; Ryan, A. J., Transformations to and from the Gyroid Phase in a Diblock Copolymer. *Macromolecules* **1998**, *31* (17), 5702-5716.
- 33. Wang, C.-Y.; Lodge, T. P., Kinetics and Mechanisms for the Cylinder-to-Gyroid Transition in a Block Copolymer Solution. *Macromolecules* **2002**, *35* (18), 6997-7006.
- 34. Dair, B. J.; Honeker, C. C.; Alward, D. B.; Avgeropoulos, A.; Hadjichristidis, N.; Fetters, L. J.; Capel, M.; Thomas, E. L., Mechanical Properties and Deformation Behavior of the Double Gyroid Phase in Unoriented Thermoplastic Elastomers. *Macromolecules* **1999**, *32* (24), 8145-8152.
- 35. Koppi, K. A.; Tirrell, M.; Bates, F. S.; Almdal, K.; Colby, R. H., Lamellae orientation in dynamically sheared diblock copolymer melts. *J. Phys. II France* **1992**, *2* (11), 1941-1959.

- 36. Kannan, R. M.; Kornfield, J. A., Evolution of Microstructure and Viscoelasticity during Flow Alignment of a Lamellar Diblock Copolymer. *Macromolecules* **1994**, *27* (5), 1177-1186.
- 37. Okamoto, S.; Saijo, K.; Hashimoto, T., REAL-TIME SAXS OBSERVATIONS OF LAMELLA-FORMING BLOCK-COPOLYMERS UNDER LARGE OSCILLATORY SHEAR DEFORMATION. *Macromolecules* **1994**, *27* (20), 5547-5555.
- 38. Oelschlaeger, C.; Gutmann, J. S.; Wolkenhauer, M.; Spiess, H. W.; Knoll, K.; Wilhelm, M., Kinetics of Shear Microphase Orientation and Reorientation in Lamellar Diblock and Triblock Copolymer Melts as Detected via FT-Rheology and 2D-SAXS. *Macromolecular Chemistry and Physics* **2007**, *208* (16), 1719-1729.
- 39. Gupta, V. K.; Krishnamoorti, R.; Chen, Z. R.; Kornfield, J. A.; Smith, S. D.; Satkowski, M. M.; Grothaus, J. T., Dynamics of Shear Alignment in a Lamellar Diblock Copolymer: Interplay of Frequency, Strain Amplitude, and Temperature. *Macromolecules* **1996**, *29* (3), 875-884.
- 40. Polis, D. L.; Smith, S. D.; Terrill, N. J.; Ryan, A. J.; Morse, D. C.; Winey, K. I., Shear-Induced Lamellar Rotation Observed in a Diblock Copolymer by in Situ Small-Angle X-ray Scattering. *Macromolecules* **1999**, *32* (14), 4668-4676.
- 41. Qiao, L.; Winey, K. I.; Morse, D. C., Dynamics of Kink Bands in Layered Liquids: Theory and in Situ SAXS Experiments on a Block Copolymer Melt. *Macromolecules* **2001**, *34* (22), 7858-7867.
- 42. Fredrickson, G. H., Steady shear alignment of block copolymers near the isotropic–lamellar transition. *Journal of Rheology* **1994**, *38* (4), 1045-1067.
- 43. Hu, H.; Gopinadhan, M.; Osuji, C. O., Directed self-assembly of block copolymers: a tutorial review of strategies for enabling nanotechnology with soft matter. *Soft Matter* **2014**, *10* (22), 3867-3889.
- 44. Chen, Z.-R.; Kornfield, J. A.; Smith, S. D.; Grothaus, J. T.; Satkowski, M. M., Pathways to Macroscale Order in Nanostructured Block Copolymers. *Science* **1997**, *277* (5330), 1248-1253.
- 45. Osuji, C. O.; Chen, J. T.; Mao, G.; Ober, C. K.; Thomas, E. L., Understanding and controlling the morphology of styrene–isoprene side-group liquid crystalline diblock copolymers. *Polymer* **2000**, *41* (25), 8897-8907.
- 46. Almdal, K.; Koppi, K. A.; Bates, F. S., Dynamically sheared body-centered-cubic ordered diblock copolymer melt. *Macromolecules* **1993**, *26* (15), 4058-4060.
- 47. Okamoto, S.; Saijo, K.; Hashimoto, T., Dynamic SAXS Studies of Sphere-Forming Block Copolymers under Large Oscillatory Shear Deformation. *Macromolecules* **1994**, *27* (14), 3753-3758.
- 48. Koppi, K. A.; Tirrell, M.; Bates, F. S.; Almdal, K.; Mortensen, K., Epitaxial growth and shearing of the body centered cubic phase in diblock copolymer melts. *Journal of Rheology (1978-present)* **1994,** *38* (4), 999-1027.
- 49. Angelescu, D. E.; Waller, J. H.; Register, R. A.; Chaikin, P. M., Shear-Induced Alignment in Thin Films of Spherical Nanodomains. *Advanced Materials* **2005**, *17* (15), 1878-1881.
- 50. Hong, Y.-R.; Adamson, D. H.; Chaikin, P. M.; Register, R. A., Shear-induced sphere-to-cylinder transition in diblock copolymer thin films. *Soft Matter* **2009**, *5* (8), 1687-1691.
- 51. Marencic, A. P.; Adamson, D. H.; Chaikin, P. M.; Register, R. A., Shear alignment and realignment of sphere-forming and cylinder-forming block-copolymer thin films. *Phys Rev E Stat Nonlin Soft Matter Phys* **2010**, *81* (1 Pt 1), 011503.
- 52. Pinna, M.; Zvelindovsky, A. V. M.; Guo, X.; Stokes, C. L., Diblock copolymer sphere morphology in ultra thin films under shear. *Soft Matter* **2011**, *7* (15), 6991-6997.
- 53. Marencic, A. P.; Wu, M. W.; Register, R. A.; Chaikin, P. M., Orientational order in sphere-forming block copolymer thin films aligned under shear. *Macromolecules* **2007**, *40* (20), 7299-7305.
- 54. Wu, M. W.; Register, R. A.; Chaikin, P. M., Shear alignment of sphere-morphology block copolymer thin films with viscous fluid flow. *Physical Review E* **2006**, *74* (4).
- 55. Zvelindovsky, A. V. M.; Sevink, G. J. A., Sphere morphology of block copolymer systems under shear. *EPL (Europhysics Letters)* **2003**, *62* (3), 370.

- 56. Stein, G. E.; Cochran, E. W.; Katsov, K.; Fredrickson, G. H.; Kramer, E. J.; Li, X.; Wang, J., Symmetry Breaking of In-Plane Order in Confined Copolymer Mesophases. *Physical Review Letters* **2007**, *98* (15), 158302.
- 57. Takagi, H.; Yamamoto, K., Phase Boundary of Frank–Kasper σ Phase in Phase Diagrams of Binary Mixtures of Block Copolymers and Homopolymers. *Macromolecules* **2019**, *52* (5), 2007-2014.
- 58. Zhang, J.; Bates, F. S., Dodecagonal Quasicrystalline Morphology in a Poly(styrene-b-isoprene-b-styrene-b-ethylene oxide) Tetrablock Terpolymer. *Journal of the American Chemical Society* **2012**, *134* (18), 7636-7639.
- 59. Lee, S.; Leighton, C.; Bates, F. S., Sphericity and symmetry breaking in the formation of Frank–Kasper phases from one component materials. *Proceedings of the National Academy of Sciences* **2014**, *111* (50), 17723-17731.
- 60. Gillard, T. M.; Lee, S.; Bates, F. S., Dodecagonal quasicrystalline order in a diblock copolymer melt. *Proceedings of the National Academy of Sciences* **2016**, *113* (19), 5167-5172.
- 61. Bates, M. W.; Lequieu, J.; Barbon, S. M.; Lewis, R. M.; Delaney, K. T.; Anastasaki, A.; Hawker, C. J.; Fredrickson, G. H.; Bates, C. M., Stability of the A15 phase in diblock copolymer melts. *Proceedings of the National Academy of Sciences* **2019**, *116* (27), 13194-13199.
- 62. Kim, K.; Arora, A.; Lewis, R. M.; Liu, M. J.; Li, W. H.; Shi, A. C.; Dorfman, K. D.; Bates, F. S., Origins of low-symmetry phases in asymmetric diblock copolymer melts. *Proceedings of the National Academy of Sciences of the United States of America* **2018**, *115* (5), 847-854.
- 63. Li, W.; Duan, C.; Shi, A.-C., Nonclassical Spherical Packing Phases Self-Assembled from AB-Type Block Copolymers. *ACS Macro Letters* **2017**, *6* (11), 1257-1262.
- 64. Dorfman, K. D., Frank–Kasper Phases in Block Polymers. *Macromolecules* **2021,** *54* (22), 10251-10270.
- 65. Matsen, M. W., Effect of Architecture on the Phase Behavior of AB-Type Block Copolymer Melts. *Macromolecules* **2012**, *45* (4), 2161-2165.
- 66. Zhang, C.; Vigil, D. L.; Sun, D.; Bates, M. W.; Loman, T.; Murphy, E. A.; Barbon, S. M.; Song, J.-A.; Yu, B.; Fredrickson, G. H.; Whittaker, A. K.; Hawker, C. J.; Bates, C. M., Emergence of Hexagonally Close-Packed Spheres in Linear Block Copolymer Melts. *Journal of the American Chemical Society* **2021**, *143* (35), 14106-14114.
- 67. Hsu, N.-W.; Nouri, B.; Chen, L.-T.; Chen, H.-L., Hexagonal Close-Packed Sphere Phase of Conformationally Symmetric Block Copolymer. *Macromolecules* **2020**, *53* (21), 9665-9675.
- 68. Imaizumi, K.; Ono, T.; Kota, T.; Okamoto, S.; Sakurai, S., Transformation of cubic symmetry for spherical microdomains from face-centred to body-centred cubic upon uniaxial elongation in an elastomeric triblock copolymer. *Journal of applied crystallography* **2003**, *36* (4), 976-981.
- 69. Sakamoto, N.; Hashimoto, T.; Han, C. D.; Kim, D.; Vaidya, N. Y., Order–Order and Order–Disorder Transitions in a Polystyrene-block-Polyisoprene-block-Polystyrene Copolymer. *Macromolecules* **1997**, *30* (6), 1621-1632.
- 70. Sakamoto, N.; Hashimoto, T., Ordering Dynamics of Cylindrical and Spherical Microdomains in Polystyrene-block-Polyisoprene-block-Polystyrene. 1. SAXS and TEM Observations for the Grain Formation. *Macromolecules* **1998**, *31* (24), 8493-8502.
- 71. Dormidontova, E. E.; Lodge, T. P., The Order–Disorder Transition and the Disordered Micelle Regime in Sphere-Forming Block Copolymer Melts. *Macromolecules* **2001**, *34* (26), 9143-9155.
- 72. Castelletto, V.; Hamley, I. W.; Holmqvist, P.; Rekatas, C.; Booth, C.; Grossmann, J. G., Small-angle X-ray scattering study of a poly(oxyphenylethylene)—poly(oxyethylene) diblock copolymer gel under shear flow. *Colloid Polym Sci* **2001**, *279* (7), 621-628.
- 73. Bang, J.; Lodge, T. P., Mechanisms and Epitaxial Relationships between Close-Packed and BCC Lattices in Block Copolymer Solutions. *The Journal of Physical Chemistry B* **2003**, *107* (44), 12071-12081.

- 74. Daniel, C.; Hamley, I. W.; Mingvanish, W.; Booth, C., Effect of shear on the face-centered cubic phase in a diblock copolymer gel. *Macromolecules* **2000**, *33* (6), 2163-2170.
- 75. Matsen, M. W., Phase Behavior of Block Copolymer/Homopolymer Blends. *Macromolecules* **1995**, 28 (17), 5765-5773.
- 76. Matsen, M. W., Stabilizing New Morphologies by Blending Homopolymer with Block Copolymer. *Physical Review Letters* **1995**, *74* (21), 4225-4228.
- 77. Matsen, M. W., Comparison of A-block polydispersity effects on BAB triblock and AB diblock copolymer melts. *Eur Phys J E Soft Matter* **2013**, *36* (4), 9857.
- 78. Wang, S.; Xie, R.; Vajjala Kesava, S.; Gomez, E. D.; Cochran, E. W.; Robertson, M. L., Close-Packed Spherical Morphology in an ABA Triblock Copolymer Aligned with Large-Amplitude Oscillatory Shear. *Macromolecules* **2016**, *49* (13), 4875-4888.
- 79. Hamley, I. W.; Pople, J. A.; Booth, C.; Yang, Y. W.; King, S. M., A Small-Angle Neutron-Scattering Study of Shear-Induced Ordering in the Cubic Phase of a Block Copolymer Gel. *Langmuir* **1998**, *14* (12), 3182-3186.
- 80. Wang, H.; Newstein, M. C.; Krishnan, A.; Balsara, N. P.; Garetz, B. A.; Hammouda, B.; Krishnamoorti, R., Ordering Kinetics and Alignment of Block Copolymer Lamellae under Shear Flow. *Macromolecules* **1999**, *32* (11), 3695-3711.
- 81. Wang, H.; Kesani, P. K.; Balsara, N. P.; Hammouda, B., Undulations and Disorder in Block Copolymer Lamellae under Shear Flow. *Macromolecules* **1997**, *30* (4), 982-992.
- 82. Meins, T.; Hyun, K.; Dingenouts, N.; Ardakani, M. F.; Struth, B.; Wilhelm, M., New Insight to the Mechanism of the Shear-Induced Macroscopic Alignment of Diblock Copolymer Melts by a Unique and Newly Developed Rheo-SAXS Combination. *Macromolecules* **2012**, *45* (1), 455-472.
- 83. Manfred, W., Fourier-Transform Rheology. *Macromolecular Materials and Engineering* **2002,** *287* (2), 83-105.
- 84. Meins, T.; Dingenouts, N.; Kubel, J.; Wilhelm, M., In Situ Rheodielectric, ex Situ 2D-SAXS, and Fourier Transform Rheology Investigations of the Shear-Induced Alignment of Poly(styrene-b-1,4-isoprene) Diblock Copolymer Melts. *Macromolecules* **2012**, *45* (17), 7206-7219.
- 85. Langela, M.; Wiesner, U.; Spiess, H. W.; Wilhelm, M., Microphase reorientation in block copolymer melts as detected via FT rheology and 2D SAXS. *Macromolecules* **2002**, *35* (8), 3198-3204.
- 86. Wang, S.; Kesava, S. V.; Gomez, E. D.; Robertson, M. L., Sustainable Thermoplastic Elastomers Derived from Fatty Acids. *Macromolecules* **2013**, *46* (18), 7202-7212.
- 87. R. H. Ewoldt, A. E. H., G. H. McKinley MITLoas: Understanding Large Amplitude Oscillatory Shear (LAOS). http://web.mit.edu/nnf/research/phenomena/mit\_laos.html.
- 88. Ewoldt, R. H.; Hosoi, A. E.; McKinley, G. H., New measures for characterizing nonlinear viscoelasticity in large amplitude oscillatory shear. *Journal of Rheology* **2008**, *52* (6), 1427-1458.
- 89. Wang, S.; Ding, W.; Yang, G.; Robertson, M. L., Biorenewable Thermoplastic Elastomeric Triblock Copolymers Containing Salicylic Acid-Derived End-Blocks and a Fatty Acid-Derived Midblock. *Macromol. Chem. Phys.* **2016**, *217* (2), 292-303.
- 90. Hyun, K.; Wilhelm, M.; Klein, C. O.; Cho, K. S.; Nam, J. G.; Ahn, K. H.; Lee, S. J.; Ewoldt, R. H.; McKinley, G. H., A review of nonlinear oscillatory shear tests: Analysis and application of large amplitude oscillatory shear (LAOS). *Progress in Polymer Science* **2011**, *36* (12), 1697-1753.
- 91. Hyun, K.; Wilhelm, M., Establishing a New Mechanical Nonlinear Coefficient Q from FT-Rheology: First Investigation of Entangled Linear and Comb Polymer Model Systems. *Macromolecules* **2009**, *42* (1), 411-422.
- 92. Hyun, K.; Baik, E. S.; Ahn, K. H.; Lee, S. J.; Sugimoto, M.; Koyama, K., Fourier-transform rheology under medium amplitude oscillatory shear for linear and branched polymer melts. *Journal of Rheology* **2007**, *51* (6), 1319-1342.

- 93. López-Barrón, C. R.; Wagner, N. J.; Porcar, L., Layering, melting, and recrystallization of a close-packed micellar crystal under steady and large-amplitude oscillatory shear flows. *Journal of Rheology* **2015**, *59* (3), 793-820.
- 94. Leblanc, J. L., Large amplitude oscillatory shear experiments to investigate the nonlinear viscoelastic properties of highly loaded carbon black rubber compounds without curatives. *Journal of Applied Polymer Science* **2008**, *109* (2), 1271-1293.
- 95. Ackerson, B. J.; Pusey, P. N., Shear-Induced Order in Suspensions of Hard Spheres. *Physical Review Letters* **1988**, *61* (8), 1033-1036.
- 96. Jiang, J.; Burger, C.; Li, C.; Li, J.; Lin, M. Y.; Colby, R. H.; Rafailovich, M. H.; Sokolov, J. C., Shear-Induced Layered Structure of Polymeric Micelles by SANS. *Macromolecules* **2007**, *40* (11), 4016-4022.
- 97. Chen, L. B.; Ackerson, B. J.; Zukoski, C. F., Rheological consequences of microstructural transitions in colloidal crystals. *Journal of Rheology* **1994**, *38* (2), 193-216.
- 98. Loose, W.; Ackerson, B. J., Model calculations for the analysis of scattering data from layered structures. *The Journal of chemical physics* **1994**, *101* (9), 7211-7220.
- 99. Martin, S.; Bryant, G.; Van Megen, W., Observation of a Smecticlike Crystalline Structure in Polydisperse Colloids. *Physical Review Letters* **2003**, *90* (25).
- 100. López-Barrón, C. R.; Porcar, L.; Eberle, A. P.; Wagner, N. J., Dynamics of melting and recrystallization in a polymeric micellar crystal subjected to large amplitude oscillatory shear flow. *Physical review letters* **2012**, *108* (25), 258301.
- 101. Kossuth, M. B.; Morse, D. C.; Bates, F. S., Viscoelastic behavior of cubic phases in block copolymer melts. *Journal of Rheology* **1999**, *43* (1), 167-196.
- 102. Sebastian, J. M.; Lai, C.; Graessley, W. W.; Register, R. A., Steady-shear rheology of block copolymer melts and concentrated solutions: Disordering stress in body-centered-cubic systems. *Macromolecules* **2002**, *35* (7), 2707-2713.
- 103. Lee, S. H.; Yong Song, H.; Hyun, K.; Hyup Lee, J., Nonlinearity from FT-rheology for liquid crystal 8CB under large amplitude oscillatory shear (LAOS) flow. *Journal of Rheology* **2014**, *59* (1), 1-19.
- 104. Scott, D. B.; Waddon, A. J.; Lin, Y. G.; Karasz, F. E.; Winter, H. H., Shear-induced orientation transitions in triblock copolymer styrene-butadiene-styrene with cylindrical domain morphology. *Macromolecules* **1992**, *25* (16), 4175-4181.
- 105. Morrison, F.; Le Bourvellec, G.; Winter, H. H., Flow-induced structure and rheology of a triblock copolymer. *Journal of Applied Polymer Science* **1987**, *33* (5), 1585-1600.